

A Family of Highly Stable Lanthanide Metal–Organic Frameworks: Structural Evolution and Catalytic Activity

Mikaela Gustafsson,^{†,‡} Agnieszka Bartoszewicz,^{†,§} Belén Martín-Matute,^{*,†,§}
Junliang Sun,^{†,‡} Jekabs Grins,^{†,‡} Tony Zhao,[§] Zhongyue Li,^{||} Guangshan Zhu,^{||} and
Xiaodong Zou^{*,†,‡}

[†]Berzelii Centre EXSELENT on Porous Materials, [‡]Inorganic and Structural Chemistry, Department of Materials and Environmental Chemistry, and [§]Organic Chemistry, Stockholm University, SE-106 91 Stockholm, Sweden, and ^{||}State Key Laboratory of Inorganic Synthesis and Preparative Chemistry, College of Chemistry, Jilin University, Changchun 130023, China

Received July 2, 2009. Revised Manuscript Received April 16, 2010

A family of homeotypic porous lanthanide metal–organic frameworks (MOFs), [Ln(btc)(H₂O)]·guest (Nd (**1**), Sm (**2**), Eu (**3**), Gd (**4**), Tb (**5**), Ho (**6**), Er (**7**), and Yb (**8**); guest: DMF or H₂O) was synthesized. The structures of the as-synthesized compounds are tetragonal and contain 1D channels with accessible lanthanide ions. In situ single crystal X-ray diffraction shows that **1** undergoes a single-crystal to polycrystalline to single-crystal transformation from room temperature to 180 °C. During the release of DMF and water molecules from the channels by evacuation and subsequent heating, the structures of **1** and **7** transformed from tetragonal to monoclinic, and then to tetragonal, while the structure of **8** remained tetragonal. The transformation between the monoclinic and the low temperature tetragonal phases is reversible. The Ln(btc) MOFs are stable to at least 480 °C and are among the most thermally stable MOFs. The Ln(btc) MOFs act as efficient Lewis acid catalysts for the cyanosilylation of aldehydes yielding cyanohydrins in high yields within short reaction times. **1** also catalyzes the cyanosilylation of less reactive substrates, such as ketones at room temperature. The Ln(btc) MOFs could be recycled and reused without loss of their crystallinity and activity.

Introduction

Porous solids constitute today an important part in the developments of functional materials in various disciplines such as heterogeneous catalysis, gas processing, sensor technology, and so forth. Metal–organic frameworks (MOFs), or coordination polymers, are constructed by metal ions/clusters that are linked by organic ligands and belong to an interesting class of functional micro- and mesoporous materials.¹ The size of periodic pores/channels in MOFs and their functionality may be altered and tuned in a systematic way by choosing suitable metal ions and organic linkers.^{1d,2} One important feature of MOFs is that they can have flexible frameworks and undergo structural changes in response to external stimuli, for example, solvent and gases, temperature, and pressure.^{1d,3}

As a result of the porous nature of MOFs and their structural flexibility, large efforts have been made toward imparting catalytic properties to MOFs for heterogeneous catalysis.⁴ Using metal ions in the framework as active centers for catalysis is one of the most common ways to generate catalytically active MOFs.⁵ Immobilization of metal complexes within the MOFs to create heterogeneous catalysts has also been reported.^{6–8} Some

*E-mail: xzou@mmk.su.se, belen@organ.su.se.

- (1) (a) James, S. L. *Chem. Soc. Rev.* **2003**, 32, 276–288. (b) Rowsell, J. L. C.; Yaghi, O. M. *Microporous Mesoporous Mater.* **2004**, 73, 3–14. (c) Rosseinsky, M. J. *Microporous Mesoporous Mater.* **2004**, 73, 15–30. (d) Férey, G. *Chem. Soc. Rev.* **2008**, 37, 191–214. (2) Yaghi, O. M.; O’Keeffe, M.; Ockwig, N. W.; Chae, H. K.; Eddaoudi, M.; Kim, J. *Nature* **2003**, 423, 705–713. (3) (a) Kitaura, R.; Fujimoto, K.; Noro, S.-I.; Kondo, M.; Kitagawa, S. *Angew. Chem., Int. Ed.* **2002**, 41, 133–135. (b) Serre, C.; Millange, F.; Thouvenot, C.; Noguès, M.; Marsolier, G.; Louër, D.; Férey, G. *J. Am. Chem. Soc.* **2002**, 124, 13519–13526. (c) Kitaura, R.; Seki, K.; Akiyama, G.; Kitagawa, S. *Angew. Chem., Int. Ed.* **2003**, 42, 428–431. (d) Serre, C.; Millange, F.; Surblé, S.; Férey, G. *Angew. Chem., Int. Ed.* **2004**, 43, 6286–6289. (e) Wu, C.-D.; Lin, W. *Angew. Chem., Int. Ed.* **2005**, 44, 1958–1961. (f) Uemura, K.; Matsuda, R.; Kitagawa, S. *J. Solid State Chem.* **2005**, 178, 2420–2429.

- (4) (a) Forster, P. M.; Cheetham, A. K. *Top. Catal.* **2003**, 24, 79–86. (b) Kesaneli, B.; Lin, W. *Coord. Chem. Rev.* **2003**, 246, 305–326. (c) Kitagawa, S.; Kitaura, R.; Noro, S.-I. *Angew. Chem., Int. Ed.* **2004**, 43, 2334–2375. (d) Schüth, F. *Annu. Rev. Mater. Res.* **2005**, 35, 209–238. (e) Ngo, H. L.; Lin, W. *Top. Catal.* **2005**, 34, 85–92. (f) Wang, Z.; Chen, G.; Ding, K. *Chem. Rev.* **2009**, 109, 322–359. (g) Farrusseng, D.; Aguado, S.; Pinel, C. *Angew. Chem., Int. Ed.* **2009**, 48, 7502–7513. (5) (a) Fuijita, M.; Kwon, Y. J.; Washizu, S.; Ogura, K. *J. Am. Chem. Soc.* **1994**, 116, 1151–1152. (b) Evans, O. R.; Ngo, H. L.; Lin, W. B. *J. Am. Chem. Soc.* **2001**, 123, 10395–10396. (c) Sato, T.; Mori, W.; Kato, C. N.; Ohmura, T.; Sato, T.; Yokoyama, K.; Takamizawa, S.; Naito, S. *Chem. Lett.* **2003**, 32, 854–855. (d) Schlögl, K.; Kratzke, T.; Kaskel, S. *Microporous Mesoporous Mater.* **2004**, 73, 81–88. (e) Alaerts, L.; Séguin, E.; Poelman, H.; Thibault-Starzyk, F.; Jacobs, P. A.; De Vos, D. E. *Chem.—Eur. J.* **2006**, 12, 7353–7363. (f) Zou, R.-Q.; Sakurai, H.; Xu, Q. *Angew. Chem., Int. Ed.* **2006**, 45, 2542–2546. (g) Nicola, C. D.; Karabach, Y. Y.; Kirillov, A. M.; Monair, M.; Pandolfo, L.; Pettinari, C.; Pombeiro, A. J. L. *Inorg. Chem.* **2007**, 46, 221–230. (h) Llabrés I Xamena, F. X.; Abad, A.; Corma, A.; Garcia, H. *J. Catal.* **2007**, 250, 294–298. (i) Llabrés I Xamena, F. X.; Casanova, O.; Tailleux, R. G.; Garcia, H.; Corma, A. *J. Catal.* **2008**, 255, 220–227. (j) Horike, S.; Dincă, M.; Tamaki, K.; Long, J. R. *J. Am. Chem. Soc.* **2008**, 130, 5854–5855. (k) Zhang, E.; Hou, H.; Han, H.; Fan, Y. *J. Organomet. Chem.* **2008**, 693, 1927–1937. (6) Wu, C.-D.; Hu, A.; Zhang, L.; Lin, W. *J. Am. Chem. Soc.* **2005**, 127, 8940–8941.

of the reported MOFs that were used as catalysts also showed size selectivity.^{9–11}

MOFs based on lanthanide ions have attracted great interest during the past decade, primarily for their luminescence and magnetic properties.^{12,13} Lanthanide-based MOFs have great potential to be excellent heterogeneous catalysts since lanthanide ions have a flexible coordination sphere and can create coordinatively unsaturated metal centers.¹⁴ There are some reports where lanthanide-based MOFs have been used as catalysts.^{15–18} In searching for new lanthanide-based MOF catalysts, we have focused our attention on a family of lanthanide MOFs constructed by seven-coordinated Ln(III) ions linked by 1,3,5-benzenetricarboxylates (BTCs). Three such isostructural MOFs have been reported, [Tb(btc)(H₂O)]·(H₂O)_{0.5}DMF (MOF-76),^{19a} [Dy(btc)(H₂O)]·DMF,^{19b} and [Eu(btc)(H₂O)]·(H₂O)_{1.5}.^{19c} These lanthanide MOFs contain 1D channels and show high thermal stability (350–500 °C). The coordinated water molecules and guest species in the channels can be removed by evacuation and heating to form permanent pores and to give coordinatively unsaturated metal centers. Recently, we have synthesized another lanthanide MOF in the family [Nd(btc)(H₂O)]·(H₂O)_{0.5}DMF (**1**). Preliminary results showed that **1** is homeotypic to the three above-mentioned lanthanide MOFs but with a different space group.²⁰ This prompted us to make a systematic study of the lanthanide MOF family and their potential as heterogeneous Lewis acid catalysts.

Here we report the synthesis, structural evolution, characterization, and catalytic activity of a series of new

homeotypic lanthanide MOFs, [Ln(btc)(H₂O)]·guest (Ln: Nd (**1**), Sm (**2**), Eu (**3**), Gd (**4**), Tb (**5**), Ho (**6**), Er (**7**), and Yb (**8**); guest: DMF (dimethylformamide) or H₂O). The lanthanide MOFs were characterized by X-ray powder diffraction (XRPD). The structures of **1** and **8** were determined in this study by single crystal X-ray diffraction, and the structures of **3** and **5** were previously reported.^{19a,c} Structural changes of **1**, **7** and **8** under evacuation and heating were further studied by in situ XRPD. The structural transformation of **1** during heating was also studied by in situ single crystal X-ray diffraction. Finally the catalytic performance of the lanthanide MOFs in terms of activity, heterogeneity, and recyclability were tested in the cyanosilylation of aldehydes and ketones.

Experimental Section

All chemicals were purchased from commercial suppliers and used without further purification.

Syntheses of [Ln(btc)(H₂O)]·guest (Ln: Nd (1**), Sm (**2**), Eu (**3**), Gd (**4**), Tb (**5**), Ho (**6**), Er (**7**), and Yb (**8**)).** A mixture of Ln(NO₃)₃·nH₂O (*n* = 5–6) (0.04 g, 1 × 10^{−4} mol), 1,3,5-benzenetricarboxylic acid (H₃BTC) (0.02 g, 1 × 10^{−4} mol), dimethylformamide (DMF) (10 mL), distilled water (2 mL), cyclohexanol (2 mL), dibutylamine (two drops), and 2 mol·L^{−1} HNO₃ (three drops) was added to a 50 mL glass beaker. The transparent solution (pH = 5) was stirred for 2 h at room temperature and placed in an oven at 85 °C for 16 h. The products, rod-like crystals of 10 × 10 × 1000 μm³ in size (**1**: purple; **2–5**, **8**: colorless; **6–7**: pink), were recovered by filtration, washed with DMF (~15 mL) and methanol (~10 mL), and finally dried at room temperature. **1–8** are stable in air, water, and common organic solvents.

Single Crystal X-ray Diffraction. Single crystal X-ray diffraction data of the as-synthesized **1** (Nd, **1**(as)) were collected at 20 °C on a Bruker SMART diffractometer equipped with a CCD camera and using Mo Kα (λ = 0.71073 Å) radiation. In situ single crystal X-ray diffraction was performed on an XCalibur3 diffractometer equipped with a CCD camera and using Mo Kα (λ = 0.71073 Å) radiation. Single crystal X-ray diffraction data of the as-synthesized **8** (Yb, **8**(as)) were collected on an MarCCD at 100 K using synchrotron radiation (λ = 0.907 Å) at the Beamline I911:5, Max Lab, Lund University, Sweden. The structures were solved and refined using the SHELX-97 program.²¹ The **1**(as) crystallizes in space group *P*₄₃ with the unit cell parameters *a* = 10.4278(4) and *c* = 14.2602(12) Å. *R*₁ = 0.0314 and *wR*₂ = 0.0572 for all 3121 unique reflections. At 180 °C, the space group of **1**(180 °C) changed to *P*₄₃22, with *a* = 10.4520(2) and *c* = 13.8486(9) Å. *R*₁ = 0.0750 and *wR*₂ = 0.0567 for all the 1509 unique reflections. **8**(as) crystallizes in space group *P*₄₁22 with *a* = 10.2410(3) and *c* = 14.4026(5) Å, *R*₁ = 0.0296 and *wR*₂ = 0.0795 for all the 1382 unique reflections. Crystallographic data and structure refinements of **1**(as), **1**(180 °C) and **8**(as) are given in the Supporting Information Table S1.

X-ray Powder Diffraction Analysis. X-ray powder diffraction (XRPD) was performed on a PANalytical X'Pert PRO diffractometer equipped with a Pixel detector and using Cu Kα₁ radiation (λ = 1.5406 Å). All samples were ground prior to data collection and dispersed uniformly on zero-background Si plates.

- (7) Alaerts, L.; Wahlen, J.; Jacobs, P. A.; De Vos, D. E. *Chem. Commun.* **2008**, 1727–1737.
- (8) Alkordi, M. H.; Liu, Y.; Larsen, R. W.; Eubank, J. F.; Eddaoudi, M. *J. Am. Chem. Soc.* **2008**, *130*, 12639–12641.
- (9) (a) Dybtsev, D. N.; Nuzhdin, A. L.; Chun, H.; Bryliakov, K. P.; Talsi, E. P.; Fredin, V. P.; Kim, K. *Angew. Chem., Int. Ed.* **2006**, *45*, 916. (b) Cho, S.-H.; Ma, B.; Nguyen, S. T.; Hupp, J. T.; Albrecht-Schmitt, T. E. *Chem. Commun.* **2006**, 2563–2565. (c) Hasegawa, S.; Horike, S.; Matsuda, R.; Furukawa, S.; Mochizuki, K.; Kinoshita, Y.; Kitagawa, S. *J. Am. Chem. Soc.* **2007**, *129*, 2607. (d) Wu, C.-D.; Lin, W. *Angew. Chem., Int. Ed.* **2007**, *46*, 1075–1078.
- (10) Seo, J. S.; Whang, D.; Lee, H.; Jun, S. I.; Oh, J.; Jeon, Y. J.; Kim, K. *Nature* **2000**, *404*, 982–986.
- (11) Zecchina, A.; Groppo, E.; Bordiga, S. *Chem.—Eur. J.* **2007**, *2*, 2440–2460.
- (12) Li, Z.; Zhu, G.; Guo, X.; Zhao, X.; Jin, Z.; Qiu, S. *Inorg. Chem.* **2007**, *46*, 5174–5178.
- (13) Guo, X.; Zhu, G.; Sun, F.; Li, Z.; Zhao, X.; Li, X.; Wang, H.; Qiu, S. *Inorg. Chem.* **2006**, *45*, 2581–2587.
- (14) Kitagawa, S.; Noro, S.-I.; Nakamura, T. *Chem. Commun.* **2006**, 701–707.
- (15) Evans, O. R.; Ngo, H. L.; Lin, W. *J. Am. Chem. Soc.* **2001**, *123*, 10395–10396.
- (16) (a) Gándara, F.; García-Cortés, A.; Cascales, C.; Gómez-Lor, B.; Gutiérrez-Puebla, E.; Monge, A. M.; Snejko, N. *Inorg. Chem.* **2007**, *46*, 3475–3484. (b) Snejko, N.; Cascales, C.; Gomez-Lor, B.; Gutiérrez-Puebla, E.; Iglesias, M.; Ruiz-Valero, C.; Monge, M. A. *Chem. Commun.* **2002**, 1366–1367. (c) Gándara, F.; de Andrés, A.; Gómez-Lor, B.; Gutiérrez-Puebla, E.; Iglesias, M.; Monge, M. A.; Proserpio, D. M.; Snejko, N. *Cryst. Growth Des.* **2008**, *8*, 378–380.
- (17) Han, J. W.; Hill, C. L. *J. Am. Chem. Soc.* **2007**, *129*, 15094–15095.
- (18) Dewa, T.; Saiki, T.; Aoyama, Y. *J. Am. Chem. Soc.* **2001**, *123*, 502–503.
- (19) (a) Rosi, N. L.; Kim, J.; Eddaoudi, M.; Chen, B.; O'Keeffe, M.; Yaghi, O. M. *J. Am. Chem. Soc.* **2005**, *127*, 1504–1518. (b) Gao, X. D.; Zhu, G. S.; Li, Z. Y.; Sun, F. X.; Yang, Z. H.; Qiu, S. L. *Chem. Commun.* **2006**, 3172–3174. (c) Chen, B.; Yang, Y.; Zapata, F.; Lin, G.; Qian, G.; Lobkovsky, E. B. *Adv. Mater.* **2007**, *19*, 1693–1696.
- (20) Gustafsson, M.; Li, Z.; Zhu, G.; Qiu, S.; Grins, J.; Zou, X. *Stud. Surf. Sci. Catal.* **2008**, *174*, 451–454.

- (21) Sheldrick, G. M. *Acta Crystallogr.* **2008**, *A64*, 112–122.

In situ XRPD data were collected from RT to 600 °C in vacuum on a PANalytical X'Pert PRO MPD diffractometer equipped with an Anton-Parr XRK900 reaction chamber, using Cu K α radiation ($\lambda = 1.5418$ Å) and variable slits. The heating rate was 2 °C/min, and the temperature was equilibrated for 2 min prior to each data collection. Measurements in vacuum (ca. 0.1 mbar) were performed using a closed Macor glass ceramic sample holder. For measurements under a nitrogen atmosphere, an open Macor glass ceramic sample holder with a sieve-like bottom (pore size 0.5 mm) was used. The temperature was controlled by a thermocouple approximately 3 mm from the sample.

High quality XRPD data of **1** (Nd) were collected with the 2θ range of 5–90° in vacuum and in situ at 25, 80, 120, and 220 °C to study the structural changes. A heating rate of 2 °C/min was used, and the temperature of the sample was equilibrated for 15 min prior to data collection. Data were collected using variable slits and 1 cm² irradiated sample area with a total measuring time of 1 h, yielding patterns with maximum peak intensities of approximately 10 000 counts. The unit cell parameters of **1**–**8** were refined from the corresponding XRPD patterns using the FullProf program.²²

Other Analyses. Thermogravimetric Analysis (TGA) was performed under a nitrogen atmosphere from 28 to 650 °C with a heating rate of 1 °C/min using a high-resolution thermogravimetric analyzer (Perkin Elmer TGA 7). Elemental analyses of C, H, and N were performed at the elemental analysis section at Santiago de Compostela University using Fisons Instruments 1108. The samples were exposed to a constant He flow before analyses. Nitrogen adsorption and desorption isotherm was measured at 77 K on a Micromeritics ASAP 2020 system. The sample was degassed at 220 °C for 6 h. FT-IR spectroscopy was performed on a Varian 670-IR spectrometer to check the coordination of the lanthanide atoms with water and the aldehyde substrate.

Catalytic Studies. Cyanosilylation of aldehydes and ketones was used for studying the catalytic performance of the Ln(btc) MOFs as Lewis acid catalysts. These studies were performed on four MOF samples **1** (Nd), **6** (Ho), **7** (Er), and **8** (Yb), which were grinded and then examined by SEM to ensure that the samples had similar particle sizes so that the effects of the particle sizes on the reactions were minimized. Samples from the same synthesis batch were used for all the catalytic experiments. A MOF sample (4.5–9.0 mol %) was activated in vacuum (0.2 mbar) at 120 °C for 4 h to generate unsaturated lanthanide metal centers and then cooled down to room temperature under a nitrogen atmosphere. Then a mixture of trimethylsilyl cyanide (TMSCN, 140 μ L, 1 mmol) and aldehyde (or ketone) (0.5 mmol) was added. The reaction mixtures were stirred at room temperature, and aliquots were taken and analyzed by ¹H NMR spectroscopy at given time intervals. Details of the catalytic experiments and analysis are given in the Supporting Information S17).

Results and Discussion

Structures of the Lanthanide MOFs. All the as-synthesized [Ln(btc)(H₂O)]·guest MOFs (**1**(as)–**8**(as)) are homeotypic, as shown by the similarity of their XRPD patterns (Supporting Information Figure S2). Single crystal X-ray diffraction shows that the structures of both **1**(as) (Nd)

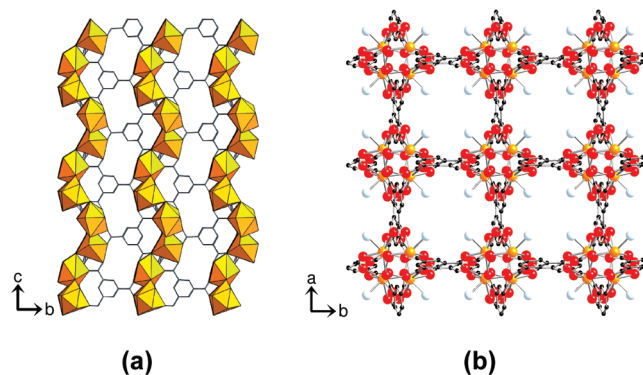


Figure 1. Crystal structure of **1** illustrating (a) chiral chains of seven-coordinated Nd clusters linked together with tridentate BTC ligands and (b) the channels (7.0×7.0 Å²) in parallel to the *c*-axis. The coordinated water molecules (light blue) are pointing toward the channel centers. Nd atoms are shown in orange, oxygen in red, and carbon in black. The DMF and uncoordinated water molecules are disordered in the channels and are not shown.

and **8**(as) (Yb) are chiral, with the space groups $P4_3$ and $P4_122$, respectively. The asymmetric unit consists of one unique Ln(III) ion and one unique BTC ligand. The Ln(III) ion is seven-coordinated and binds to six oxygen atoms from six different BTC ligands and one water molecule (Supporting Information Figure S1c). Each BTC ligand binds to six different Ln(III) ions. The LnO₆-(H₂O) polyhedra are located around the $4_1/3$ axis and connected by corner-sharing to form chiral –Ln–O–C–O–Ln– chains along the *c*-axis (Figure 1). These chains are linked together via the BTC ligands in the *a*- and *b*-directions to form a 3D framework, with channels running along the *c*-axis. The coordinated water molecules point toward the channels. Although each crystal exhibits only one hand, the sample is not in an enantiopure form. The chemical formulas deduced from the elemental analysis are [Nd(btc)(H₂O)]·(H₂O)_{0.5}DMF for **1** (observed (wt %): C 31.4, H 2.8, N 3.0; calculated (wt %): C 31.9, H 2.9, N 3.1) and [Yb(btc)(H₂O)]·(H₂O)_{0.5}(DMF)_{0.6} for **8** (observed: C 27.4%, H 2.2%, N 1.9%; calculated C 28.8%, H 2.3%, N 1.9%). The DMF and uncoordinated water molecules are disordered in the channels. All water and DMF molecules can be removed upon heating. The free diameter of the channel is about 7.0×7.0 Å², if the water and DMF molecules are removed.

The unit cell parameters of the different [Ln(btc)(H₂O)]·guest MOFs obtained from the XRPD data are compared to the ionic radii²³ for the corresponding Ln(III) ions (Figure 2 and Supporting Information Table S2). The *a*- (and *b*-) parameters decrease linearly with decreasing ionic radius of the Ln(III) ion (giving shorter Ln–O distances), which in turn decreases with increasing atomic number.²⁴ However, a similar trend is not observed for the *c*-parameter, which increases from Nd to Gd and then decreases. The structures of **1** (Nd) and **8** (Yb) refined

(23) Shannon, R. D. *Acta Crystallogr.* **1976**, *A32*, 751–767.

(24) (a) Gerkin, R. E.; Reppart, W. J. *Acta Crystallogr.* **1984**, *C40*, 781–786. (b) Chatterjee, A.; Maslen, E. N.; Watson, K. J. *Acta Crystallogr.* **1988**, *B44*, 381–386. (c) Quadrelli, E. A. *Inorg. Chem.* **2002**, *41*, 167–169.

(22) Rodriguez-Carjaval, J. *FULLPROF*, Version 3.2.; ILL: Grenoble, 2005.

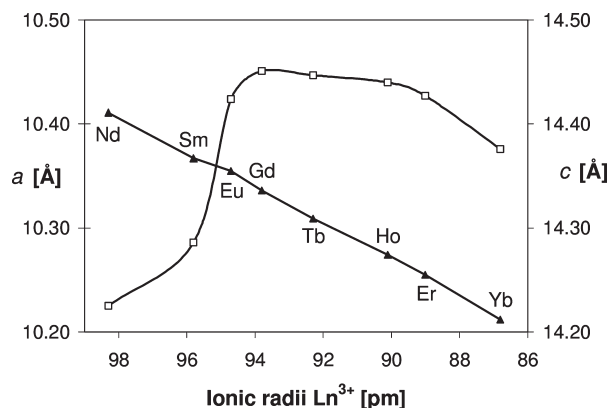


Figure 2. Unit cell parameters a (▲) and c (□) of **1–8** obtained from XRPD, compared with the ionic radii of Ln(III) ions. The a parameter decreases linearly with the increasing ionic radius. The c parameter increases first from **1** (Nd) to **4** (Gd) and then decreases from **4** (Gd) to **8** (Yb). The standard deviations of the unit cell parameters are between 0.001 and 0.003 Å.

from single crystal X-ray diffraction data show that the Yb–O distances (2.26(1) Å) are shorter compared with those of the Nd–O distances (2.40(8) Å), resulting in the shorter a - and b -axes. The longer c -axis for **8** compared to that for **1** is due to the larger O–Yb–O angles (165.4(4)°, O3–Yb–O3) compared to the corresponding O–Nd–O angles (154.7(2)°, O2–Nd–O4) along the c -axis.

Structural Changes during Evacuation and Heating. In situ XRPD showed that **1** (Nd) undergoes structural changes upon removal of the DMF and water molecules, from tetragonal to monoclinic and then back to tetragonal. The structure of **1**(as) started to change prior to the heating as soon as vacuum (ca. 0.1 mbar) was applied (Figure 3). The structure was finally stabilized after 2 h leading to a second phase with a significant change in the XRPD pattern (**1**(25 °C), Figure 3). Subsequent heating to 80 °C resulted in only minor shifts of the peak positions (**1**(80 °C), Figure 3). At 120 °C, **1**(80 °C) transformed completely to a third phase, **1**(120 °C) (Figure 3). A fourth phase (**1**(220 °C)) started to form above 120 °C and the phase transformation finally completed at 220 °C. Further heating only resulted in some minor shifts of the peak positions to high angles.

The unit cell parameters refined from the XRPD patterns at different temperatures (Table 1) show that **1**(as) transformed from tetragonal to monoclinic (**1**(25 °C)) within 15 min when vacuum was applied. The major change was the γ angle, from 90.0° to 106.5°. The c -parameter decreased by 0.44 Å, from 14.22 to 13.78 Å, while the a -parameter only decreased slightly (<0.12 Å). Only minor changes were observed when the sample was heated

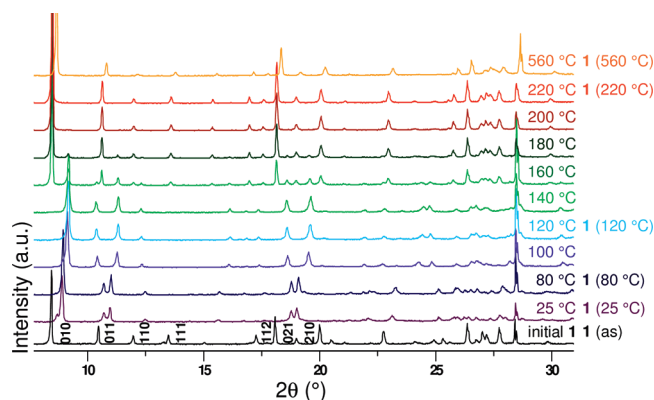


Figure 3. In situ XRPD patterns of **1** heated in vacuum. The peaks were shifted to high angles, and the intensities of the weak reflections (110), (111), and (112) decreased significantly once the vacuum was applied. In addition some peaks (for example, (011) and (210)) were split into two. No further changes were observed after the sample had been in vacuum for 2 h. The XRPD pattern was further changed upon heating. The structure changed from tetragonal (**1**(as)) to monoclinic (**1**(25 °C), **1**(80 °C), and **1**(120 °C)) and finally back to tetragonal (**1**(220 °C)). The tetragonal phase was stable up to 560 °C. The pattern at 160 °C is a mixture of **1**(220 °C) (main phase) and **1**(120 °C) (minor phase).

up to 80 °C. The XRPD pattern recorded at 120 °C could be indexed by a monoclinic phase, **1**(120 °C), with a larger γ angle (111.0°) and a shorter c -parameter (13.37 Å) compared to those of **1**(80 °C). The unit cell volume decreased by 14% from **1**(as) to **1**(120 °C) (Table 1). The monoclinic phase **1**(120 °C) transformed to a tetragonal phase **1**(220 °C) upon heating from 120 to 220 °C. The transformation was completed at this temperature. Further heating to 560 °C only gave a small contraction of the unit cell (Figure 3) and no significant structural changes were observed.

It is important to know if the phase transformation led to significant structural changes of the framework since they may change the coordination environment of the Ln(III) ions. In situ high quality XRPD data of **1**(as), **1**(80 °C), **1**(120 °C), and **1**(220 °C) were collected at 25, 80, 120, and 220 °C, respectively, to identify the structural changes. The XRPD data allowed us to locate the positions of the Nd(III) ions, while the positions of the BTC and the coordinated water molecules could only be determined approximately. Unfortunately, it was not possible to perform reliable structure refinements on the XRPD data due to the large scattering difference between the Nd(III) and the BTC molecules.

In situ X-ray diffraction on a single crystal of **1** was then performed to determine the structural changes. The crystal was heated in air from room temperature to 180 °C, and the diffraction was monitored simultaneously. To our surprise, the reflections almost disappeared when the crystal was heated to 80 °C and then came back at 180 °C.

Table 1. Unit Cell Parameters of **1** in Air, in Vacuum, and at Different Temperatures, from in Situ XRPD Data

phases	temperature [°C]	a [Å]	b [Å]	c [Å]	γ [deg]	V [Å ³]
1	25 (no vacuum)	10.411(2)	10.411(2)	14.225(3)	90	1542
1 (25 °C)	25 (vacuum)	10.291(3)	10.327(3)	13.777(8)	106.47(1)	1404
1 (80 °C)	80	10.2869(5)	10.2873(5)	13.7604(4)	106.644(3)	1395
1 (120 °C)	120	10.318(1)	10.3017(8)	13.3739(8)	110.99(2)	1328
1 (220 °C)	220	10.473(1)	10.4735(7)	13.832(2)	90	1517
1 (560 °C)	560	10.460(1)	10.460(1)	13.851(2)	90	1484

After three hours of preheating at 180 °C to ensure a complete structural transformation, single crystal X-ray diffraction data were collected at this temperature. The high-temperature phase **1** (180 °C) has a similar structure compared to **1(as)** but with a higher symmetry ($P4_322$ instead of $P4_3$). The BTC ligands within the framework were slightly rotated compared to those in **1(as)**. The coordinated water molecules were removed (Supporting Information Figure S1). Our study shows that **1** underwent a single-crystal to polycrystalline to single-crystal transformation upon the release of the DMF and water molecules from the channels. When the crystal was cooled down to room temperature, the reflections disappeared, due to the rehydration of the sample.

PXRD showed that the high temperature structure was retained when the activated sample was cooled down to room temperature, as long as the sample is in vacuum. The sample lost its crystallinity upon rehydration in air in less than 10 min. Interestingly, the crystallinity was completely recovered in less than 20 min after a few drops of DMF were added to the sample (Supporting Information Figure S3). This implies that the addition of the organic solvent facilitates the rearrangement of the metal and BTC molecules and stabilizes the MOF structures.

The major structural changes during evacuation and heating occurred below 180 °C, which is most probably due to the rearrangement of the framework associated with the release of the DMF and water molecules from the channels. This agrees with that observed in the XRPD patterns where peak intensities decreased significantly during this process. The structure was stabilized and became more ordered after all water and DMF molecules were removed, so that the intensities of the diffraction peaks increased and the peaks became sharper. The diffraction of **1** could be observed by X-ray powder diffraction but not by single crystal X-ray diffraction during heating from room temperature to 180 °C. This is probably associated with that the tetragonal unit cell can be transformed into the monoclinic unit cells by four different ways, which may result in small twin domains in the monoclinic crystal.

The thermal behaviors of **7** (Er) and **8** (Yb) (Supporting Information Figures S4 and S5) were to some extent different from those of **1** (Nd). **7(as)** was transformed first to a tetragonal superstructure at 80 °C ($a(80\text{ °C}) \approx \sqrt{2}a(\text{as})$), then to a monoclinic phase between 100 and 160 °C and finally to a tetragonal phase at 180 °C (Supporting Information Table S3). The decrease of the unit cell volume from **7(as)** to **7(120 °C)** was only 4.7%, much smaller than the corresponding decrease of **1(as)** (14%). The monoclinic angle of **7(120 °C)** is 100.2°, also much smaller than that of **1(120 °C)**, 111.0°. The structural changes of **8** were much less compared to those of **1** and **7**; **8** remained tetragonal throughout the heating to at least 500 °C (Supporting Information Table S4).

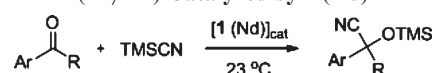
The in situ XRPD shows that **1**, **7**, and **8** were stable to at least 500–550 °C (Figure 3 and Supporting Information Figures S4–S5). They are among the MOFs that have the highest thermal stability.

Thermogravimetric Analysis (TGA). Thermogravimetric analyses of **1** (Nd) and **8** (Yb) showed weight losses in several steps from 28 to 600 °C (Supporting Information Figure S6). The total weight loss of **1** before 280 °C corresponds to the loss of all water and DMF molecules. **1** started to lose its BTC molecules at 480 °C and consequently the structure started to collapse. We noticed that the temperatures at which the different molecules started to leave **1** are different from those observed by in situ XRPD. This may be due to the different heating rate and different atmosphere used in the two experiments. **8** has a slightly higher thermal stability than **1**, and started to lose the BTC molecules at 500 °C. The nitrogen adsorption and desorption study of **1** degassed at 220 °C for 6 h shows that it is a microporous solid with the Type I isotherm (Supporting Information Figure S7). FT-IR spectroscopy on a sample of **1** showed that water molecules were removed after the MOF was activated at 120 °C for 3 h (Supporting Information Figure S11).

Catalytic Tests. To compare the catalytic properties of our compounds with other MOFs, we choose the cyanosilylation of aldehydes and ketones (Scheme 1). The Lewis acid-catalyzed reaction of carbonyl compounds with cyanide affords the highly versatile cyanohydrin trimethylsilyl ethers. Cyanohydrins can be readily converted into important compounds such as α -hydroxycarboxylic acids or β -amino alcohols.²⁵ The **1** (Nd) catalyst (9.0 mol % for aldehydes and 4.5 mol % for ketones) was activated at 120 °C under vacuum (0.2 mbar) for 4 h to generate coordinatively unsaturated Nd(III) centers and subsequently cooled down to room temperature under a nitrogen atmosphere. A solution of aldehyde (or ketone) (0.5 mmol) and TMSCN (1 mmol) was then added. TMSCN acted here both as a reagent and as the solvent; no other solvent was used. The reaction mixture was stirred at room temperature under a nitrogen atmosphere for the time indicated, and aliquots were taken and analyzed by ¹H NMR spectroscopy (Supporting Information Figure S15).

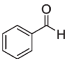
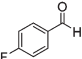
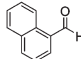
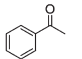
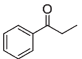
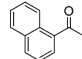
The catalyst **1** shows very high activity in the cyanosilylation of benzaldehyde and 88% conversion was reached in only 1 h (Table 2, entry 1). A high conversion was also obtained in 2 h (99%) when CH₂Cl₂ was used as the solvent. The catalyst **1** showed a higher activity in the

Scheme 1. Cyanosilylation of Aldehydes (R = H) or Ketones (R \neq H) Catalyzed by **1 (Nd)**



- (25) For some examples, see: (a) Matthews, B. R.; Gountzos, H.; Jackson, W. R.; Watson, K. G. *Tetrahedron Lett.* **1989**, 30, 5157–5158. (b) Ziegler, T.; Hörsch, B.; Effenberger, F. *Synthesis* **1990**, 575–578. (c) Jackson, W. R.; Jacobs, H. A.; Jayatilake, G. S.; Matthews, B. R.; Watson, K. G. *Aust. J. Chem.* **1990**, 43, 2045–2062. (d) Jackson, W. R.; Jacobs, H. A.; Matthews, B. R.; Jayatilake, G. S.; Watson, K. G. *Tetrahedron Lett.* **1990**, 31, 1447–1450. (e) Effenberger, F.; Stelzer, U. *Angew. Chem., Int. Ed.* **1991**, 30, 873–874. (f) Kim, S. S.; Song, D. H. *Eur. J. Org. Chem.* **2005**, 1777–1780.

Table 2. Cyanosilylation of Aldehydes and Ketones Catalyzed by **1** (Nd)^{a,b}

Entry	1	2	3	4	5	6
Carbonyl substrate						
Time (h)	1	1	1	18	18	18
Yield of cyanohydrin (%) ^c	88 ^b	73	18	91	80	16

^aThe yields were determined by ¹H NMR spectroscopy (Figure S15). ^b99% yield in 2 h with solvent CH₂Cl₂.

cyanosilylation of benzaldehyde than that obtained with other MOFs,^{5a,b,d,j} the Mn MOF catalyst reported by Long et al.^{5j} afforded 98% conversion of benzaldehyde after 9 h at room temperature when using 11 mol % catalyst loading. Removal of **1** by filtration shut down the reaction completely, and no significant increase of the conversion of benzaldehyde was observed after 72 h (Supporting Information Table S5), as shown in a control experiment using 4.5 mol % of the catalyst **1**. This demonstrates that the homogeneous species was not involved in the catalysis, and the catalyst **1** did not leach Nd(III) ions into the solution under the reaction conditions. The catalyst could be recycled and reused for at least five times without losing the activity (Supporting Information Table S6), giving rise to a total TON of 111. FT-IR spectroscopy and XRPD showed that benzaldehyde interacted with coordinatively unsaturated Nd(III) centers (Supporting Information Figures S13 and S14). An excellent result was also obtained for *p*-fluorobenzaldehyde (73% conversion in 1 h, Table 2, entry 2). When a larger α -naphthaldehyde was used, a significantly lower yield (18%) was obtained (Table 2, entry 3).

The cyanosilylation of benzaldehyde was also carried out with catalysts **6** (Ho), **7** (Er), and **8** (Yb). As shown in Table 3, the activity of the Ln(btc) catalysts decreases with the ionic radius of the Ln(III) ions, in an order of **1**, **6**, **7**, and **8**. **1** and **6** showed much higher activity, with 99% and 76% conversions in 2 h, respectively, while **7** and **8** afforded lower yields (61% and 57%, respectively) even after extended reaction times (5 h, Table 3). This trend is opposite to that observed for homogeneous lanthanide triflate (Ln(OTf)₃) catalysts, where the relative Lewis acidities of Ln(III) increases in an order of Nd(III), Ho(III), Er(III), and Yb(III).^{26,27} The observed decrease in reactivity of the Ln(btc) catalysts with the ionic radius may be due to the increased steric interactions of the substrates when approaching the coordinatively unsaturated Ln(III) ions in the framework. XRPD shows that under the catalytic conditions, the structure of **1** was monoclinic while the structures of **6**, **7**, and **8** were close to tetragonal (Supporting Information Figures S8 and

Table 3. Cyanosilylation of Benzaldehyde Catalyzed by a Variety of Ln(btc) MOFs^a

entry	MOF	yield (%)	time (h)	TON
1	1 (Nd)	99	2	22
2	6 (Ho)	76	2	17
		99	3	
3	7 (Er)	61	5	14
4	8 (Yb)	57	5	13

^aThe corresponding aldehyde (0.5 mmol) and TMSCN (1 mmol) were added to the activated Ln(btc) MOF (4.5 mol %) in CH₂Cl₂ at room temperature. The reaction mixture was stirred under nitrogen atmosphere for the time indicated.

S9). All the catalysts could be recycled and reused at least five times without losing their activity (Supporting Information Table S6) and crystallinity (Supporting Information Figure S10).

Ketones are much less reactive than aldehydes. The cyanosilylation catalyzed by **1** (4.5 mol %) at room temperature for 18 h gave excellent yields for acetophenone (91%, Table 2, entry 4). This conversion is much higher than those obtained by other MOFs (the Mn MOF gave 28% conversion of acetophenone in 24 h with 11 mol % catalyst loading at room temperature).^{5j} A high yield was also obtained for propiophenone (Table 2, entry 5), whereas a low yield was obtained for a larger ketone (Table 2, entry 6). **1** is the first example of MOFs that catalyzes the cyanosilylation of ketones with high yields in a reasonable reaction time.

Conclusions

We have synthesized a series of homeotypic [Ln(btc)(H₂O)]·guest MOFs. The structure is tetragonal and contains 1D channels. The guest and coordinated water molecules can be easily removed by heating to give Ln(btc) MOFs with micropores and coordinatively unsaturated Ln(III) centers. During the evacuation and subsequent heating, the structures of **1** and **7** transform from tetragonal to monoclinic, and then to tetragonal, while **8** remains tetragonal. The transformation between the monoclinic and the low temperature tetragonal phases is reversible. **1** undergoes a single-crystal (tetragonal) to polycrystalline (monoclinic) to single-crystal (tetragonal) transformation when being heated from room temperature to 180 °C. The transformation between the monoclinic and the low temperature tetragonal phases is reversible. The Ln(btc) MOFs are stable up to at least 480 °C and are among the most thermally stable MOFs.

- (26) (a) Imamoto, T.; Nishiura, M.; Yamanoi, Y.; Tsuruta, H.; Yamaguchi, K. *Chem. Lett.* **1996**, 875–876. (b) Tsuruta, H.; Imamoto, T.; Yamaguchi, K. *Chem. Commun.* **1999**, 1703–1704. (c) Yamanaka, M.; Nishida, A.; Nakagawa, M. *Org. Lett.* **2000**, 2, 159–161.
 (27) For an investigation of the catalytic effect of Lewis acids in water, see: Kobayashi, S.; Nagayama, S.; Busujima, T. *J. Am. Chem. Soc.* **1998**, 120, 8287–8288.

Our Ln(btc) MOFs catalyze the cyanosilylation of aldehydes and ketones in good to excellent yields within short reaction times. The catalysis is completely heterogeneous and can occur under solvent-free conditions at room temperature. The catalysts can be recycled and reused without loss of their activity and crystallinity. As a result of their high thermal stability, we believe that new applications of these materials will be soon developed.

Acknowledgment. Assoc. Prof. Niklas Hedin is acknowledged for his advice with the N_2 sorption measurement. Prof. Janos Mink is acknowledged for evaluating the FT-IR

spectra. This project is supported by the Swedish Research Council (VR) and the Swedish Governmental Agency for Innovation Systems (VINNOVA) through the Berzelii Center EXSELENT, the Göran-Gustafsson Foundation and the Ministry of Education of China through the “111” program.

Supporting Information Available: Crystallographic data and refinement parameters for **1**, **1**(180 °C) and **8**, the corresponding cif files, XRPD and in situ XRPD patterns, TGA curves, nitrogen sorption isotherm, FT-IR spectra, general procedures for the catalytic experiments and tests, and ^1H NMR spectra (PDF, CIF). This material is available free of charge via the Internet at <http://pubs.acs.org>.